Phenomenological template family for black-hole coalescence waveforms

P. Ajith[1], S. Babak[2], Y. Chen[2], M. Hewitson[1], B. Krishnan[2], J. T. Whelan[2], B. Brügmann[3], P. Diener[4,5], J. Gonzalez[3], M. Hannam[3], S. Husa[3], M. Koppitz[2], D. Pollney[2], L. Rezzolla[2,5], L. Santamaría[3], A. M. Sintes[2,6], U. Sperhake[3], and J. Thornburg[2,7]

[1] Max-Planck-Institut für Gravitationsphysik (Albert-Einstein-Institut) and Leibniz Universität Hannover, Callinstr. 38, 30167 Hannover, Germany
[2] Max-Planck-Institut für Gravitationsphysik (Albert-Einstein-Institut), Am Mühlenberg 1, 14476 Golm, Germany
[3] Theoretisch-Physikalisches Institut, Friedrich Schiller Universität Jena, Max-Wien-Platz 1, 07743 Jena, Germany
[4] Center for Computation & Technology, Louisiana State University, Baton Rouge, LA, USA
[5] Department of Physics and Astronomy, Louisiana State University, Baton Rouge, LA, USA
[6] Departament de Física, Universitat de les Illes Balears, Cra. Valldemossa Km. 7.5, E-07122 Palma de Mallorca, Spain
[7] School of Mathematics, University of Southampton, Southampton SO17 1BJ, England

Abstract.

Recent progress in numerical relativity has enabled us to model the non-perturbative merger phase of the binary black-hole coalescence problem. Based on these results, we propose a phenomenological family of waveforms which can model the inspiral, merger, and ring-down stages of black hole coalescence. We also construct a template bank using this family of waveforms and discuss its implementation in the search for signatures of gravitational waves produced by black-hole coalescences in the data of ground-based interferometers. This template bank might enable us to extend the present inspiral searches to higher-mass binary black-hole systems, *i.e.*, systems with total mass greater than about 80 solar masses, thereby increasing the reach of the current generation of ground-based detectors.

1. Introduction

The first generation of ground-based gravitational wave detectors [1, 2, 3] are currently operating at unprecedented levels of sensitivity and the LIGO detectors, in particular, have attained their design goals over a broad frequency range. The data from these detectors has been used to search for a wide variety of gravitational-wave sources including coalescing binary black-hole systems (see *e.g.*, [4, 5]). In parallel with these experimental and observational achievements, a series of breakthroughs has occurred in numerical simulations of binary black hole systems [6, 7, 8]. Long-term evolutions of inspiralling black holes that last for several orbits have been obtained with several independent codes [9, 10, 11, 12, 13, 14, 15, 16], and accurate gravitational-wave signals have been

computed. It is now possible, in principle, to use these numerical-relativity results in astrophysical searches for gravitational waves. However, the high computational cost of these simulations makes it unfeasible to numerically generate all the necessary waveforms to cover the parameter space that needs to be searched. It is therefore necessary, at the present time, to use results from post-Newtonian (PN) theory to extend the waveforms obtained from numerical relativity (NR). The issue of matching NR and PN waveforms for equal-mass binary black-hole systems, and using numerical relativity results in gravitational-wave searches has been considered previously [17, 18, 19, 20]. We generalize this to unequal mass systems and suggest a phenomenological template bank parametrized only by the masses of the two individual black holes. This template bank could be used to search for binary black-hole signals in data from current and future generations of gravitational-wave detectors. Our phenomenological approach is motivated by the work of Buonanno *et al* [21], but using only *physical* parameters and generalized to include recent results from numerical relativity.

In this paper we combine *restricted* 3.5PN waveforms [22] with results from NR simulations to construct *"hybrid"* waveforms for the quasi-circular inspiral of non-spinning binaries with possibly unequal masses. Restricting ourselves to the leading-order quadrupole modes, we find that the hybrid waveforms can be approximated by phenomenological analytical waveforms with fitting factors ≥ 0.99 in the total mass range between 30 and 130 $M_{\odot}$ for Initial LIGO [23]. For our analysis we use numerical waveforms obtained with two independent codes: *(i)* long waveforms (12 cycles) from equal mass binaries, provided by the AEI-CCT groups, using their CCATIE code [24] based on the Cactus framework [25] and Carpet mesh-refinement driver [26]; *(ii)* waveforms from an unequal mass parameter study presented by the Jena group in [27], which have been obtained with the BAM code [13]. An analysis of these waveforms focusing on ring-down and higher modes has been presented in [28].

The rest of this paper is organized as follows: Section 2 summarizes the numerical simulations and how numerical waveforms have been computed. In Section 3 hybrid waveforms are produced by matching PN and NR waveforms. In Section 4, we propose a family of phenomenological waveforms in the Fourier domain, and study their impact for detection and parameter estimation by computing the fitting factors of the phenomenological waveforms with the hybrid ones. We also parametrize the best-matched phenomenological waveforms in terms of the physical parameters. Section 5 shows the astrophysical range of a search using the full coalescence waveforms and a preliminary comparison with other searches. Finally, Section 6 concludes with a summary of our results and plans for future work.

2. Numerical simulations

Both the BAM [13] and CCATIE [24] codes are finite-difference mesh-refinement codes solving the Einstein equations within the "moving puncture" framework [7, 8, 29, 16].

In the wave-zone, sufficiently far away from the source, the spacetime metric can be accurately described as a perturbation of a flat background metric; let h_{ab} denote the metric perturbation where a, b denote spacetime indices. Let t be the time coordinate used in the numerical simulation to foliate the spacetime by spatial slices. Working, as usual, in the transverse-traceless (TT) gauge, all the information about the radiative degrees of freedom is contained in the spatial part h_{ij} of h_{ab}, where i, j denote spatial indices. Let us use a coordinate system (x, y, z) on a spatial slice so that the z-axis is along the total angular momentum of the binary system at the starting time. Let ι be the inclination

angle from the z-axis, and let ϕ be the phase angle and r the radial distance coordinates so that (r, ι, ϕ) are standard spherical coordinates in the wave-zone.

Working in the TT gauge, the radiative degrees of freedom in h_{ab} can be written, as usual, in terms of two polarizations h_+ and $h_\times$:

$$h_{ij} = h_+ (\mathbf{e}_+)_{ij} + h_\times (\mathbf{e}_\times)_{ij}, \tag{1}$$

where $\mathbf{e}_{+,\times}$ are the usual basis tensors for TT tensors in the wave frame

$$(\mathbf{e}_+)_{ij} = \hat{\iota}_i \hat{\iota}_j - \hat{\phi}_i \hat{\phi}_j \,, \qquad \text{and} \qquad (\mathbf{e}_\times)_{ij} = \hat{\iota}_i \hat{\phi}_j + \hat{\iota}_j \hat{\phi}_i \,. \tag{2}$$

Here $\hat{\iota}$ and $\hat{\phi}$ are the unit vectors in the ι and ϕ directions respectively. The wave, of course, propagates in the radial direction.

In our numerical simulations, the gravitational waves are extracted by two distinct methods. The first one uses the Newman-Penrose Weyl tensor component Ψ_4 (see e.g. [30]) which, in an appropriate gauge, is a measure of the outgoing transverse gravitational radiation in an asymptotically flat spacetime. In the wavezone it can be written in terms of the complex strain $\mathsf{h} = h_+ - \mathrm{i} h_\times$ as [31],

$$\mathsf{h} = \lim_{r\to\infty} \int_0^t \mathrm{d}t' \int_0^{t'} \mathrm{d}t'' \Psi_4. \tag{3}$$

An alternative method for wave extraction, which has a long history in numerical relativity, determines the waveform via gauge-invariant perturbations of a background Schwarzschild spacetime, via the Zerilli-Moncrief formalism (see [32] for a review). In terms of the even ($Q^{(+)}_{\ell m}$) and odd ($Q^{(\times)}_{\ell m}$) parity master functions, the gravitational wave strain amplitude is then given by

$$\mathsf{h} = \frac{1}{\sqrt{2}r} \sum_{l,m} \left(Q^+_{\ell m} - \mathrm{i} \int_{-\infty}^t Q^\times_{\ell m}(t') \mathrm{d}t' \right) Y^{-2}_{\ell m} + \mathcal{O}\left(\frac{1}{r^2}\right). \tag{4}$$

Results from the BAM code have used the Weyl tensor component Ψ_4 and Eq. (3), with the implementation described in [13]. While the CCATIE code computes waveforms adopting both methods, the AEI-CCT waveforms used here were computed using the perturbative extraction and Eq. (4). At an appropriate extraction radius, the two methods for determining h are found to agree very well for moving-puncture black-hole evolutions of the type considered here [16].

It is useful to discuss gravitational radiation fields in terms of spin-weighted $s = -2$ spherical harmonics $Y^s_{\ell m}$, and in this paper we will only consider the dominant $\ell = 2$, $m = \pm 2$ modes (see [28] for the higher ℓ contribution in the unequal mass case), with basis functions

$$Y^{-2}_{2-2} \equiv \sqrt{\frac{5}{64\pi}} \, (1 - \cos\iota)^2 \, e^{-2\mathrm{i}\phi}, \quad Y^{-2}_{22} \equiv \sqrt{\frac{5}{64\pi}} \, (1 + \cos\iota)^2 \, e^{2\mathrm{i}\phi}. \tag{5}$$

Our "input" NR waveforms correspond to the projections

$$\mathsf{h}_{\ell m} \equiv \langle Y^{-2}_{\ell m}, \mathsf{h} \rangle = \int_0^{2\pi} \mathrm{d}\phi \int_0^\pi \mathsf{h} \, \overline{Y^{-2}_{\ell m}} \, \sin\iota \, \mathrm{d}\iota \,, \tag{6}$$

of the complex strain h, where the bar denotes complex conjugation. In the cases considered here, we have equatorial symmetry so that $\mathsf{h}_{22} = \overline{\mathsf{h}_{2-2}}$, and

$$\mathsf{h}(t) = \sqrt{\frac{5}{64\pi}} e^{2\mathrm{i}\phi} \left((1 + \cos\iota)^2 \, \mathsf{h}_{22}(t) + (1 - \cos\iota)^2 \, \bar{\mathsf{h}}_{22}(t) \right). \tag{7}$$

In practice, we choose $\iota = 0$, thus $\mathsf{h}(t) = 4\sqrt{\frac{5}{64\pi}} \, \mathsf{h}_{22}(t) \approx 0.631 \, \mathsf{h}_{22}(t)$.

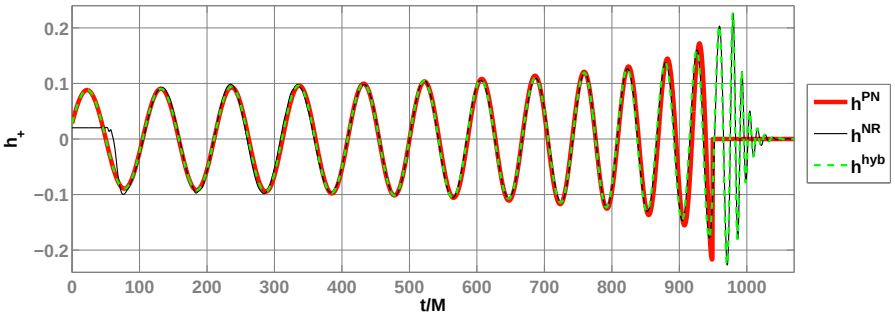

Figure 1. NR waveform (black) from an equal-mass simulation, along with the 'best-matched' 3.5PN waveform (red). The Hybrid waveform constructed from the above is also shown (dashed line).

3. Matching post-Newtonian and numerical relativity waveforms

Once the PN and NR waveforms are generated, we produce a set of hybrid waveforms by matching them in an overlapping time interval $t_1 \leq t < t_2$. The obvious assumption in this procedure is that such an overlapping region exists and that in it both approaches yield the correct waveforms.

Each time-domain waveform $h(t, \boldsymbol{\mu})$ is parametrized by a vector $\boldsymbol{\mu} = \{M, \eta, \phi_0, t_0\}$, where $M \equiv m_1 + m_2$ is the total-mass of the binary, $\eta \equiv m_1 m_2/(m_1 + m_2)^2$ is the symmetric mass-ratio, ϕ_0 is the initial phase and t_0 is the start time of the waveform. We match the PN waveforms $h^{\rm PN}_{+,\times}(t, \boldsymbol{\mu})$ and the NR waveforms $h^{\rm NR}_{+,\times}(t, \boldsymbol{\nu})$ ‡ by minimizing the square difference between the respective polarizations. *i.e.*,

$$\delta \equiv \min_{\boldsymbol{\mu}, a} \left[\sum_{i=+,\times} \int_{t_1}^{t_2} \left[h_i^{\rm PN}(t, \boldsymbol{\mu}) - a\, h_i^{\rm NR}(t, \boldsymbol{\nu}) \right]^2 {\rm d}t \right]. \tag{8}$$

The minimization is carried over the parameters $\boldsymbol{\mu}$ of the PN waveform and an amplitude scaling factor a §. The hybrid waveforms are produced by combining the 'best-matched' PN waveforms and the NR waveforms in the following way:

$$h^{\rm hyb}_{+,\times}(t, \boldsymbol{\nu}) \equiv \begin{cases} h^{\rm PN}_{+,\times}(t, \boldsymbol{\mu}_0) & \text{if } t < t_1 \\ a_0\, \tau\, h^{\rm NR}_{+,\times}(t, \boldsymbol{\nu}) + (1-\tau)\, h^{\rm PN}_{+,\times}(t, \boldsymbol{\mu}_0) & \text{if } t_1 \leq t < t_2 \\ a_0\, h^{\rm NR}_{+,\times}(t, \boldsymbol{\nu}) & \text{if } t_2 \leq t \end{cases} \tag{9}$$

where $\boldsymbol{\mu}_0$ and a_0 denote the values of $\boldsymbol{\mu}$ and a for which δ is minimum, and $\tau = (t - t_1)/(t_2 - t_1)$ is a linearly-increasing weighting function, such that $0 \leq \tau < 1$.

An example set of hybrid waveforms is shown in Fig. 1. The numerical waveform (black line) from an equal-mass ($\eta = 0.25$) simulation by the AEI-CCT group is matched with a 3.5PN inspiral waveform (red line) over the matching region $100M \leq t < 850M$. The hybrid waveform (dashed line) is constructed by combining the above as per Eq.(9).

‡ The parameters $\boldsymbol{\nu}$ are taken from the same set as $\boldsymbol{\mu}$, but with different values.

§ The amplitude scaling factor was introduced in order to accommodate possible errors in the amplitude of the NR waveforms due to, for example, the finite radius of the extraction sphere. The best-matched value of a, however, was found to be 1 ± 0.08.

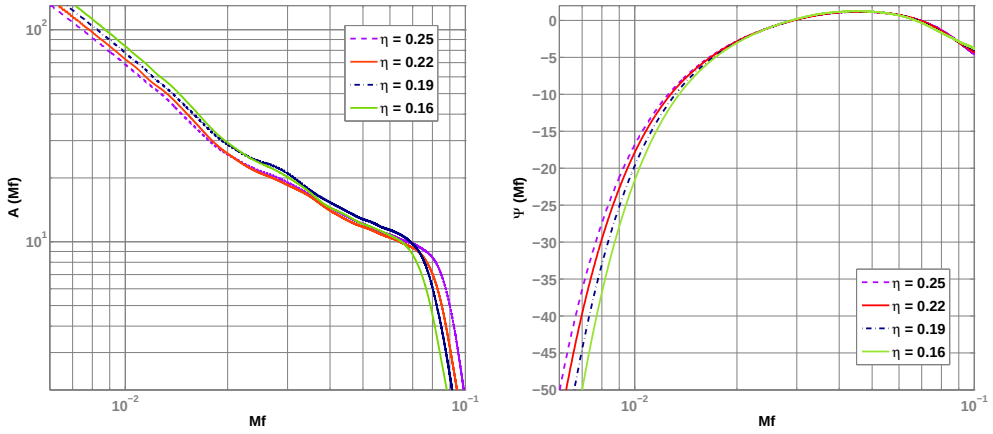

Figure 2. Fourier domain magnitude (left) and phase (right) of the hybrid waveforms. Symmetric mass-ratio η of each waveform is shown in the legends.

The robustness of the matching procedure can be tested by computing the overlaps between hybrid waveforms constructed with different matching regions. If the overlaps are very high, this can be taken as an indication of the robustness of the matching procedure. A more detailed discussion of this will be presented in [33].

Fig. 2 shows the hybrid waveforms of different mass-ratios in the Fourier domain. In particular, the panel on the left shows the amplitude of the waveforms in the Fourier domain, while the panel on the right shows the phase. These waveforms are constructed by matching 3.5PN waveforms with the NR waveforms from the unequal mass ($0.16 \leq \eta \leq 0.25$) simulations by the Jena group. In the next section, we try to parametrize these Fourier domain waveforms in terms of a set of phenomenological parameters.

4. The phenomenological template bank

An obvious issue when using the above constructed hybrid waveforms directly as detection templates is that it might be computationally very expensive to compute enough NR waveforms to cover the entire parameter space densely enough. In this section, we propose a phenomenological waveform family which has more than 99 % overlaps with the hybrid waveforms in the detection band of the Initial LIGO detectors. We also show how this phenomenological waveform family can be mapped to the physical parameters (M and η), so that the template bank, at the end, is two-dimensional.

4.1. Phenomenological waveforms

We write our phenomenological waveform in the Fourier domain as

$$u(f) \equiv \mathcal{A}_{\rm eff}(f)\, {\rm e}^{{\rm i}\Psi_{\rm eff}(f)}. \tag{10}$$

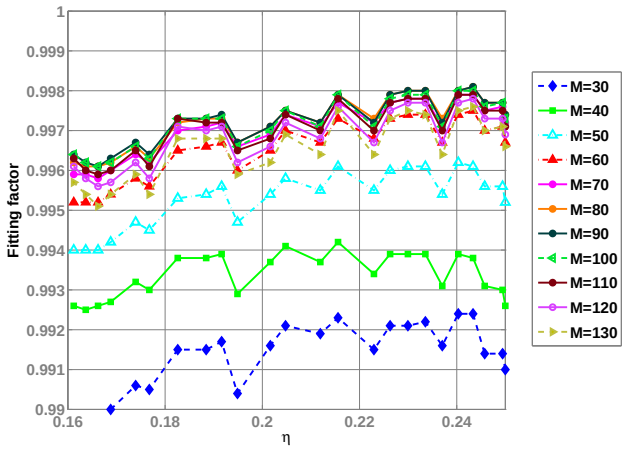

Figure 3. Fitting factors of the hybrid waveforms with the phenomenological waveform family. Horizontal axis shows the symmetric mass ratio of the binary, while different colours/markers correspond to different total masses.

where $\mathcal{A}_{\rm eff}(f)$ is the amplitude of the waveform in the frequency domain, which we choose to write in terms of a set of *"amplitude parameters"* $\boldsymbol{\alpha} = \{f_{\rm merg}, f_{\rm ring}, f_{\rm cut}, \sigma\}$ as

$$\mathcal{A}_{\rm eff}(f) \equiv \begin{cases} (f/f_{\rm merg})^{-7/6} & \text{if } f < f_{\rm merg} \\ (f/f_{\rm merg})^{-2/3} & \text{if } f_{\rm merg} \leq f < f_{\rm ring} \\ w\,\mathcal{L}(f, f_{\rm ring}, \sigma) & \text{if } f_{\rm ring} \leq f < f_{\rm cut} \end{cases} \tag{11}$$

In the above expression,

$$\mathcal{L}(f, f_{\rm ring}, \sigma) \equiv \left(\frac{1}{2\pi}\right) \frac{\sigma}{(f - f_{\rm ring})^2 + \sigma^2/4}\,, \tag{12}$$

represents a Lorentzian function of width σ centered around $f_{\rm ring}$. The normalisation constant w is chosen in such a way that $\mathcal{A}_{\rm eff}(f)$ is continuous across the "transition" frequency $f_{\rm ring}$, *i.e.*,

$$w \equiv \frac{\pi\sigma}{2} \left(\frac{f_{\rm ring}}{f_{\rm merg}}\right)^{-2/3}\,, \tag{13}$$

where we use $f_{\rm cut}$ as the cutoff frequency of the template and $f_{\rm merg}$ as the frequency at which the power-law changes from $f^{-7/6}$ to $f^{-2/3}$ (as noted previously in [17] for the equal-mass case).

Taking our motivation from the stationary-phase expansion of the gravitational-wave phase, we write the effective phase $\Psi_{\rm eff}(f)$ as an expansion in powers of f.

$$\Psi_{\rm eff}(f) = 2\pi f t_0 + \phi_0 + \psi_0\, f^{-5/3} + \psi_2\, f^{-1} + \psi_3\, f^{-2/3} + \psi_4\, f^{-1/3} + \psi_6\, f^{1/3}\,, \tag{14}$$

where t_0 is the time of arrival, ϕ_0 is the frequency-domain phase offset, and $\boldsymbol{\beta} = \{\psi_0, \psi_2, \psi_3, \psi_4, \psi_6\}$ are the *"phase parameters"*, that is the set of phenomenological parameters describing the phase of the waveform.

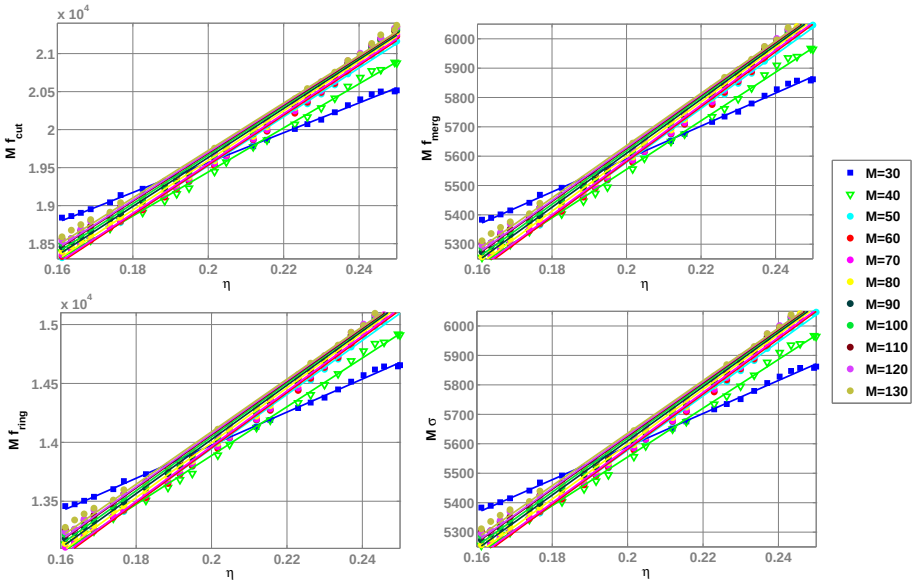

Figure 4. Best-matched amplitude parameters $\boldsymbol{\alpha}_{\rm max}$ in terms of the physical parameters of the binary. The horizontal axis shows the symmetric mass-ratio of the binary and different colors/markers correspond to different total masses. Linear polynomial fits to the data points are also shown.

The fitting factors [34] of the hybrid waveforms with the family of phenomenological waveforms are shown in Fig. 3 over the parameter range of $30 \leq M/M_{\odot} \leq 130$ and $0.16 \leq \eta \leq 0.25$, using the Initial LIGO noise spectrum. It is quite apparent that the fitting factors are almost always greater than 0.99, thus underlining the effectiveness of the phenomenological waveforms in reproducing the hybrid ones.

4.2. From phenomenological to physical parameters

It is possible to reparametrise the best-matched phenomenological waveforms in terms of the physical parameters of the hybrid waveforms. In Fig. 4, we plot the amplitude parameters $\boldsymbol{\alpha}_{\rm max}$ of the best-matched phenomenological waveforms against the physical parameters of the binary. Similarly, the phase parameters $\boldsymbol{\beta}_{\rm max}$ of the best-matched phenomenological waveforms are plotted against the physical parameters of the binary in Fig. 5. The linear polynomial fits to the data points serve as a numerical "look-up table" to go from the physical parameters $\{M, \eta\}$ to the best-matched phenomenological parameters $\{\boldsymbol{\alpha}_{\rm max}, \boldsymbol{\beta}_{\rm max}\}$. Thus the template bank lives on a two-dimensional manifold (parametrised by M and η) embedded in a higher-dimensional space.

It might be worth stressing that the search will be carried out over M and η, and *not* over the phenomenological parameters. The phenomenological parameters $\boldsymbol{\alpha}$ and $\boldsymbol{\beta}$, are constrained by the numerical look-up tables (see Figs. 4 and 5), and only serve as an intermediate step in generating the template waveforms.

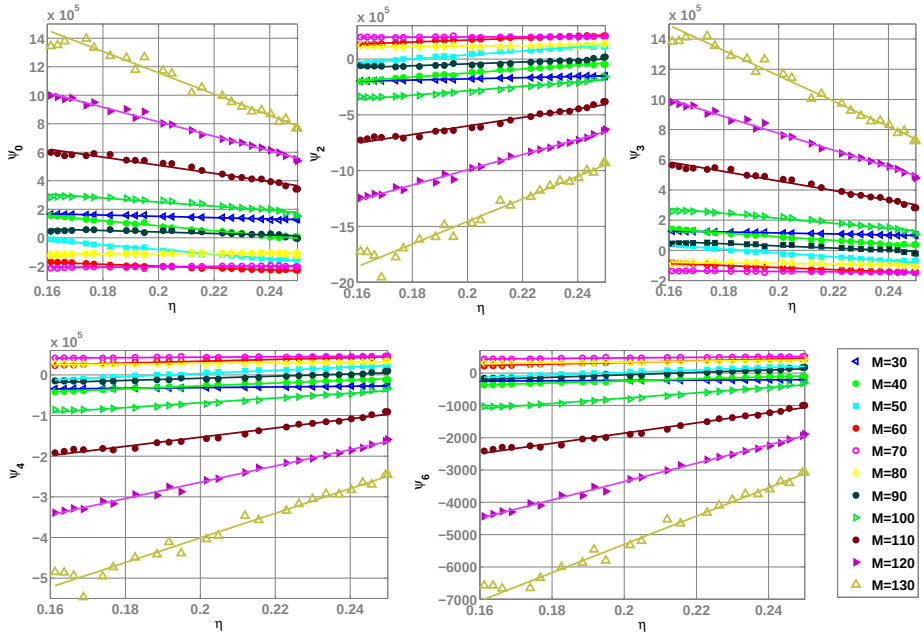

Figure 5. The same as in Fig. 4 but for the phase parameters $\boldsymbol{\beta}_{\max}$.

5. The astrophysical range and comparison with other searches

The template family proposed in this paper can be used for coherently searching for all the three stages (inspiral, merger, and ring-down) of the binary coalescence, thus making this potentially more sensitive than searches which look at the three stages separately. Fig. 6 compares the sensitivity of the searches using different template families. What is plotted here is the distance at which an optimally-oriented, equal-mass binary would produce an optimal signal-to-noise ratio (SNR) of 8 at the Initial LIGO noise spectrum. The dotted line corresponds to a search using PN templates truncated at the Schwarzschild innermost stable circular orbit (ISCO), the dashed line corresponds to a search using ring-down templates [35], and the solid line to a search using all three stages of the binary coalescence using the template bank proposed here. The horizontal axis reports the total-mass of the binary, while the vertical axis the distance in Mpc. It is quite evident that, for binaries with $50 \leq M/M_{\odot} \leq 140$, the "coherent search" using the new template family is, theoretically, more than twice as sensitive as any other search considered here. In a forthcoming paper [33], we will extend this comparison to include other approaches which model all the three stages of black hole coalescence such as, for example [36].

However, while this looks promising, we emphasize that it is important to treat Fig. 6 as only a preliminary assessment; fitting factors are not the only consideration for a practical search strategy. It is also very important to consider issues which arise when dealing with real data. For example, false alarms produced by noise artifacts, might well determine the true sensitivity of the search, and these artifacts will inevitably be present in real data. This is however beyond the scope of the present work, and further investigation is required before we can properly assess the efficacy of our phenomenological template bank in real-life searches.

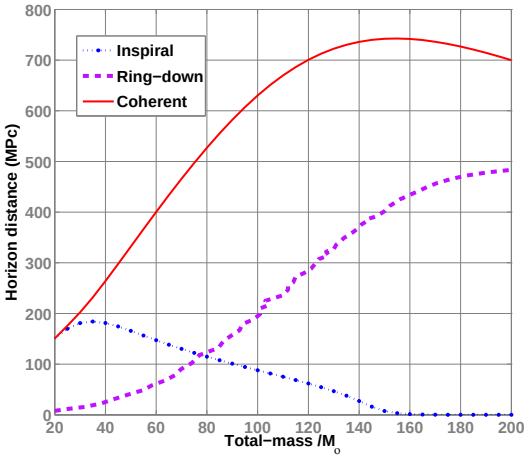

Figure 6. A preliminary assessment of the phenomenological template bank. This figure plots, as a function of the total mass, the distance to an optimally-oriented binary which can produce an optimal SNR of 8 at the Initial LIGO noise spectrum. The dotted line corresponds to a search using PN templates truncated at ISCO, the dashed line corresponds to a search using ring-down templates (from [35]), and the solid line corresponds to a search using the template family proposed in this paper.

6. Summary and outlook

Making use of the recent results from numerical relativity we have proposed a phenomenological waveform family which can model the inspiral, merger and ring-down stages of binary black-hole coalescence. We first constructed a set of hybrid waveforms by matching the NR waveforms with the analytical PN waveforms. Then, we analytically constructed phenomenological waveforms which approximated the hybrid waveforms. The family of phenomenological waveforms that we propose was found to have fitting factors larger than 0.99 with the hybrid waveforms in the detection band of Initial LIGO. We have also shown how this phenomenological waveform family can be parametrized in terms of the physical parameters (M and η) of the binary, so that the template bank is, at the end, two dimensional. This phenomenological waveform family can be used to densely cover the parameter space, avoiding the computational cost of generating numerical waveforms at every grid point in the parameter space. We have also compared the sensitivity of a search using this template family with other searches. This search might enable us to extend the mass-range of the present inspiral searches to higher mass ($> 80\,M_\odot$) systems. In the mass-range $50\,M_\odot$ to $140\,M_\odot$, this search could be significantly more sensitive than the search using the standard PN inspiral templates and quasi-normal mode ring-down templates.

The numerical "look-up tables" to go from the physical parameters to the phenomenological parameters (see Figs. 4 and 5) can be replaced by analytical functions of M and η. This makes it easier to compute the parameter space metric used for template placement [37] and will be studied in future work. Our plans for future work also include the study of the robustness of the matching procedure used to construct the hybrid waveforms by considering different matching regions and PN waveforms of different order, and of course, to eventually construct a realistic search pipeline which incorporates

numerical relativity waveforms in gravitational wave searches.

Acknowledgments

NR computations were performed with the Belladonna and Peyote clusters of the Albert Einstein Institute, the Doppler and Kepler clusters of the Jena group, and at LRZ Munich and HLRS, Stuttgart. This work was supported in part by DFG grant SFB/Transregio 7 "Gravitational Wave Astronomy". The Jena group thanks the DEISA Consortium (co-funded by the EU, FP6 project 508830), for support within the DEISA Extreme Computing Initiative (www.deisa.org). AMS gratefully acknowledges the support of the Spanish Ministerio de Educación y Ciencia research project FPA-2004-03666 and the Albert Einstein Institute and the University of Jena for hospitality. PD thanks the Albert Einstein Institute for hospitality. The PN waveforms were generated using the LSC Algorithms Library (LAL), and numerical data-analysis calculations were performed with the aid of Merlin, Morgane and Zeus clusters of the Albert Einstein Institute.

References

[1] S. J. Waldman (for the LIGO Science Collaboration), *Class. Quantum Grav.* **23**, S653-S660 (2006).
[2] S. Hild (for the LIGO Scientific Collaboration), *Class. Quantum Grav.* **23**, S643-S651 (2006).
[3] F. Acernese *et al* , *Class. Quantum Grav.* **23**, S635-S642 (2006).
[4] B. Abbott *et al* (The LIGO Scientific Collaboration), *Phys. Rev. D* **73**, 062001 (2006).
[5] B. Abbott *et al* (The LIGO Scientific Collaboration), arXiv:0704.3368 [gr-qc].
[6] F. Pretorius, *Phys. Rev. Lett.* **95**, 121101 (2005).
[7] M. Campanelli, C. O. Lousto, P. Marronetti, and Y. Zlochower, *Phys. Rev. Lett.* **96**, 111101 (2006).
[8] J. G. Baker *et al* , *Phys. Rev. Lett.* **96**, 111102 (2006).
[9] F. Pretorius, *Class. Quantum Grav.* **23**, S529–S552 (2006).
[10] M. Campanelli, C. O. Lousto, and Y. Zlochower, *Phys. Rev. D* **73**, 061501(R) (2006).
[11] J. G. Baker *et al* , *Phys. Rev. D* **73**, 104002 (2006).
[12] U. Sperhake, (2006). gr-qc/0606079.
[13] B. Brügmann *et al* , (2006) gr-qc/0610128.
[14] M. A. Scheel *et al* , *Phys. Rev. D* **74**, 104006 (2006).
[15] F. Herrmann, I. Hinder, D. Shoemaker, P. Laguna, R. A. Matzner, (2007). gr-qc/0701143.
[16] M. Koppitz *et al* , (2007). gr-qc/0701163.
[17] A. Buonanno, G.B. Cook, and F. Pretorius, (2006). gr-qc/0610122.
[18] T. Baumgarte *et al* , (2006). gr-qc/0612100.
[19] J. G. Baker *et al* , (2006). gr-qc/0612024.
[20] Y. Pan *et al* , (2007). arXiv:0704.1964[gr-qc].
[21] A. Buonanno, Y. Chen and M. Vallisneri *Phys. Rev.D* **67** 024016 (2003).
[22] L. Blanchet, T. Damour, G. Esposito-Farese, B. R. Iyer, *Phys. Rev. Lett.* **93**, 091101 (2004).
[23] A. A. Abramovici *et al* , *Science* **256**, 325–333 (1992).
[24] M. Alcubierre *et al* , *Phys. Rev. D* **67**, 084023 (2003).
[25] `http://www.cactuscode.org`.
[26] E. Schnetter, S. H. Hawley and I. Hawke, *Class. Quant. Grav.* **21**, 1465 (2004).
[27] J. A. González *et al* , *Phys. Rev. Lett.* **98**, 091101 (2007).
[28] E. Berti *et al* , (2007). gr-qc/0703053.
[29] M. Hannam, S. Husa, D. Pollney, B. Brügmann, and N. Ó. Murchadha, (2006). gr-qc/0606099.
[30] J. Stewart, *Advanced General Relativity*, Cambridge Monographs on Mathematical Physics.
[31] S. A. Teukolsky, *Astrophys. J.* **185**, 635 (1973).
[32] A. Nagar and L. Rezzolla, *Class. Quant. Grav.* **22**, R167 (2005) [Erratum-ibid. **23**, 4297 (2006)].
[33] P. Ajith *et al* , In preparation (2007).
[34] T. A. Apostolatos, *Phys. Rev. D* **52** 605620 (1995).
[35] L. M. Goggin (for the LIGO Scientific Collaboration), *Class. Quantum Grav* **23**, S709S713 (2006).
[36] A. Buonanno and T. Damour, *Phys. Rev. D* **59**, 084006 (1999).
[37] B. J. Owen, *Phys. Rev. D* **53** 6749-6761 (1996).